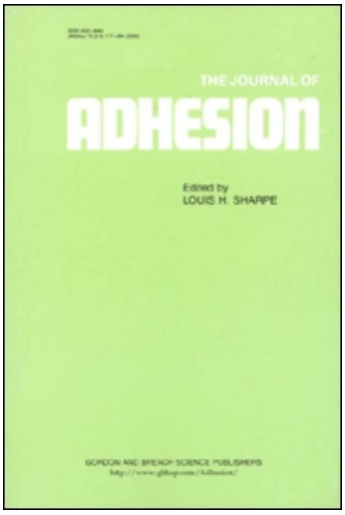

The Journal of Adhesion
Publication details, including instructions for authors and subscription information:
http://www.informaworld.com/smpp/title~content=t713453635

A Two-dimensional Stress Analysis of Butt Adhesive Joints Having a Circular Hole Defect in the Adhesive Subjected to External Bending Moments

K. Temma[a]; T. Sawa[b]; H. Uchida[b]; Y. Nakano[c]
[a] Department of Mechanical Engineering, Kisarazu National College of Technology, Chiba, Japan [b] Department of Mechanical Engineering, Yamanashi University, Yamanashi, Japan [c] Department of Mechanical Engineering, Sagami Institute of Technology, Kanagawa, Japan

To cite this Article Temma, K. , Sawa, T. , Uchida, H. and Nakano, Y.(1991) 'A Two-dimensional Stress Analysis of Butt Adhesive Joints Having a Circular Hole Defect in the Adhesive Subjected to External Bending Moments', The Journal of Adhesion, 33: 3, 133 — 147
To link to this Article: DOI: 10.1080/00218469108030423
URL: http://dx.doi.org/10.1080/00218469108030423

J. Adhesion, 1991, Vol. 33, pp. 133–147
Reprints available directly from the publisher
Photocopying permitted by license only

Printed in the United Kingdom

A Two-dimensional Stress Analysis of Butt Adhesive Joints Having a Circular Hole Defect in the Adhesive Subjected to External Bending Moments

K. TEMMA,

Department of Mechanical Engineering, Kisarazu National College of Technology, Chiba, Japan

T. SAWA* and H. UCHIDA

Department of Mechanical Engineering, Yamanashi University, 4-3-11 Takeda, Kofu, Yamanashi, 400 Japan

Y. NAKANO,

Department of Mechanical Engineering, Sagami Institute of Technology, Kanagawa, Japan

(Received October 30, 1989; in final form August 7, 1990)

This paper deals with a two-dimensional stress analysis of butt adhesive joints, with a circular hole defect in the adhesive, subjected to external bending moments. The analysis was done using the two-dimensional theory of elasticity in order to examine the strength of the joints. It was assumed that the adherends were rigid and the adhesive was replaced with a finite strip including a hole defect. The effects of the location and size of a hole defect on the stress distributions around the hole and at the interfaces were obtained by numerical calculations. In addition, the singular stress near the edge of the interface was obtained. For verification, photoelastic experiments were performed. The analytical results were fairly consistent with the experimental results. It was seen that the principal stress around a hole becomes larger with a certain shift toward the free boundary. It was also seen that the stress concentration became larger with an increase of the size of the hole.

KEY WORDS Elasticity; stress analysis; butt adhesive joints; bending moment; photoelasticity; circular hole; defect; stress singularity.

1 INTRODUCTION

Adhesive joints have been used in mechanical structures with the development of modern structural adhesives. Adhesive joints have many attractive features including, (i) stress concentration does not appear because there is no hole

* Corresponding author.

present, unlike bolted or riveted joints (ii) it is possible to join different materials easily. But adhesive joints have not been used in principal load-bearing parts of structures, because of large deviations in the strength of the adhesive. Until now, adhesive joints have been designed empirically. However, data are now available for the establishment of an optimal design method. Up to now, some investigations have been carried out on lap, scarf and butt adhesive joints using the finite element method,[1–3] and the theory of elasticity.[4–7] In most of these analytical investigations, the joints were considered to contain no defects, such as a small hole or a fillet in and at the ends of the adhesive. In the process of making adhesive joints, defects such as the hole and the fillet mentioned above often occur. These defects are thought to be one of the reasons for the deviation in the measured strength of adhesive joints. However, the effect of these defects on the stress distributions and the strength of the joints have not been fully elucidated, to our knowledge, except for butt adhesive joints having a circular hole in the adhesive subjected to external tensile loads[8] and lap joints having multiple flaws.[9] A thorough investigation of the impact of defects is needed in order to establish an optimal design method for adhesive joints.

The purpose of this study is to clarify the effect of a circular hole in an adhesive on the stress distributions of butt adhesive joints subjected to external bending moments. Two assumptions are made; i) The two adherends are assumed to be rigid thin plates, and ii) The adhesive layer has a circular hole defect. The stress distributions in the joint are analyzed using a two-dimensional theory of elasticity and an iteration method to satisfy the boundary conditions of the adhesive layer and the hole periphery sufficiently. Furthermore, the effects of the location and size of a hole on the stress distributions are clarified by numerical calculations and photoelastic experiments.

2 THEORETICAL ANALYSIS

Figure 1 shows a butt adhesive joint subjected to an external bending moment M in which two similar thin plates, hereafter called the adherends (II), are bonded by an adhesive (I) with a circular hole of radius a at the position (x_0, y_0). The width and the thickness of adhesive (I) are designated by $2l$ and $2h$, and its Young's modulus and Poisson's ratio are E and ν, respectively. In the analysis, each adherend (II) is assumed to be a rigid plate of semi-infinite length and of the same width as the adhesive (I). The boundary conditions on the adhesive are expressed by Eqs. (1) and (2), and that at the hole periphery is expressed by Eq. (3).

$$\sigma_x = 0, \qquad \tau_{xy} = 0 \quad (x = \pm l) \tag{1}$$

$$v = \frac{\varepsilon_0}{l} x, \qquad \frac{\partial u}{\partial x} = 0 \quad (y = \pm h) \tag{2}$$

$$\sigma_r = 0, \qquad \tau_{r\theta} = 0 \quad (r = a) \tag{3}$$

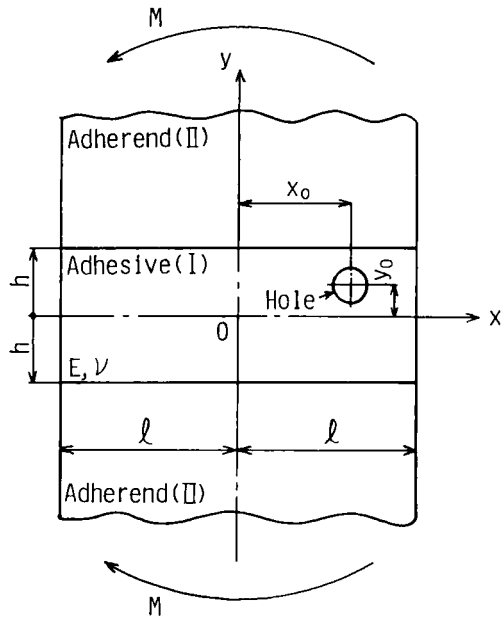

FIGURE 1 A butt adhesive joint with a circular hole subjected to an external bending moment.

where, σ_x and σ_r denote the normal stresses, τ_{xy} and $\tau_{r\theta}$ the shear stresses, and u and v the displacements in the x- and y-directions, respectively, and ε_0 denotes the maximum displacement at $x = l$ and $y = h$. M is given by the equation

$$M = \int_{-l}^{l} \sigma_{y\,|\,y=\pm h} \cdot x \, dx.$$

Plane stress conditions are assumed. A solution which satisfies the equations (1)–(3) is obtained using Schwartz's alternating method of the following analytical steps.

Step 1. The stress distribution on the joint, which contains no circular hole in the adhesive under the boundary conditions (1) and (2), is solved analytically using the two-dimensional theory of elasticity. The stress distributions σ_r and $\tau_{r\theta}$ at the hole periphery ($r = a$) are obtained analytically from this solution.

Step 2. In order to satisfy Eq. (3), the stresses equivalent to σ_r and $\tau_{r\theta}$ obtained in Step 1, are added reversely to the adhesive(I) such that the stresses at the hole periphery are eliminated. In this step, the stresses and the displacements are expressed as the following equations (4) and (5) using Airy's stress function ψ in polar coordinates.[10]

$$\left.\begin{aligned} \sigma_r &= \frac{1}{r}\frac{\partial \psi}{\partial r} + \frac{1}{r^2}\frac{\partial^2 \psi}{\partial \theta^2} \\ \sigma_\theta &= \frac{\partial^2 \psi}{\partial r^2} \\ \tau_{r\theta} &= \frac{1}{r^2}\frac{\partial \psi}{\partial \theta} - \frac{1}{r}\frac{\partial^2 \psi}{\partial r\, \partial \theta} \end{aligned}\right\} \tag{4}$$

$$\left.\begin{aligned} 2Gu &= -\frac{\partial \psi}{\partial r} + \frac{1}{1+\nu} r \frac{\partial \phi}{\partial \theta} \\ 2Gv &= -\frac{1}{r}\frac{\partial \psi}{\partial \theta} + \frac{1}{1+\nu} r^2 \frac{\partial \phi}{\partial r} \end{aligned}\right\} \tag{5}$$

where

$$\nabla^4 \psi = 0, \qquad \nabla^2 \phi = 0, \qquad \nabla^2 \psi = \frac{\partial^2 (r\phi)}{\partial r \, \partial \theta}$$

$$\nabla^2 = \frac{\partial^2}{\partial r^2} + \frac{1}{r}\frac{\partial}{\partial r} + \frac{1}{r^2}\frac{\partial^2}{\partial \theta^2}$$

and G is the shear modulus of the adhesive ($G = E/2(1+\nu)$).

Generally, the stress function ψ for an infinite plate including a circular hole as shown in Fig. 2(a), is expressed as the following Eq. (6). Moreover, Eq. (7) is

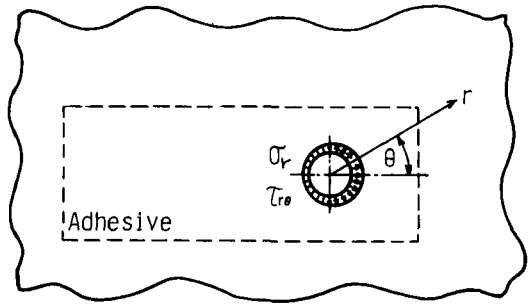

(a)

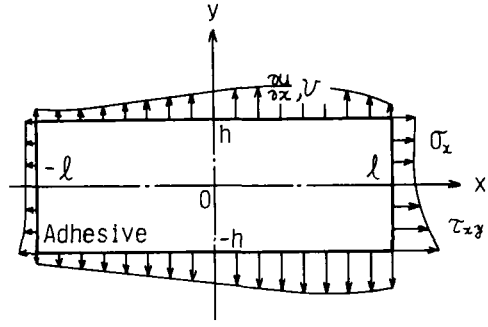

(b)

FIGURE 2 Model for analysis of adhesive.

obtained from Eqs. (4) and (6).

$$\psi = A_0\theta + B_0 \log r + A_1 r \log r \cos\theta + B_1 r\theta \sin\theta + C_1 r\theta \cos\theta + D_1 r \log r \sin\theta + \sum_{n=2}^{\infty} \{A_n r^{-n} + B_n r^{-n+2}) \cos(n\theta) + \sum_{n=2}^{\infty} \{C_n r^{-n} + D_n r^{-n+2}\} \sin(n\theta) \tag{6}$$

$$\left.\begin{aligned} \sigma_r &= \frac{B_0}{r^2} + \left(\frac{A_1}{r} + \frac{2B_1}{r}\right)\cos\theta + \left(\frac{D_1}{r} - \frac{2C_1}{r}\right)\sin\theta \\ &\quad - \sum_{n=2}^{\infty} \{n(n+1)A_n r^{-n-2} + (n-1)(n+2)B_n r^{-n}) \cos(n\theta) \\ &\quad - \sum_{n=2}^{\infty} \{n(n+1)C_n r^{-n-2} + (n-1)(n+2)D_n r^{-n}\} \sin(n\theta) \\ \tau_{r\theta} &= \frac{A_0}{r^2} + \frac{A_1}{r}\sin\theta - \frac{D_1}{r}\cos\theta - \sum_{n=2}^{\infty} \{n(n+1)A_n r^{-n-2} \\ &\qquad + n(n-1)B_n r^{-n}\} \sin(n\theta) \\ &\quad + \sum_{n=2}^{\infty} \{n(n+1)C_n r^{-n-2} + n(n-1)D_n r^{-n}\} \cos(n\theta) \end{aligned}\right\} \tag{7}$$

In these equations, A_0, $A_1, \ldots, A_n$, B_n, C_n, and D_n $(n = 1, 2, 3, \ldots)$ are unknown coefficients. They are determined by comparing the coefficients in Eq. (7) with those of the stresses $(-\sigma_r, -\tau_{r\theta})$ added to the adhesive (I), and transformed into Fourier series. The stress distributions σ_x and τ_{xy} and the deviation $\partial u/\partial x$ of displacement and the displacement v are generated again at the boundary of adhesive (I) $(x = \pm l,\ y = \pm h)$, as shown in Fig. 2(b), and they are expressed by using the stress function ψ and Eqs. (4) and (5).

Step 3. Again, in order to satisfy Eqs. (1) and (2), the stresses and the displacements contradicting those generated in Step 2, must be added to adhesive (I). In this step, the stresses and the displacements are expressed as the following equations (8) and (9) using Airy's stress function χ in rectangular coordinates[10]:

$$\sigma_x = \frac{\partial^2\chi}{\partial y^2}, \qquad \sigma_y = \frac{\partial^2\chi}{\partial x^2}, \qquad \tau_{xy} = -\frac{\partial^2\chi}{\partial x\,\partial y} \tag{8}$$

$$2Gu = -\frac{\partial\chi}{\partial x} + \frac{1}{1+\nu}\frac{\partial\phi}{\partial y}, \qquad 2Gv = -\frac{\partial\chi}{\partial y} + \frac{1}{1+\nu}\frac{\partial\phi}{\partial x} \tag{9}$$

where

$$\nabla^4\chi = 0, \qquad \nabla^2\phi = 0, \qquad \nabla^2\chi = \frac{\partial^2\phi}{\partial x\,\partial y} \left(\nabla^2 = \frac{\partial^2}{\partial x^2} + \frac{\partial^2}{\partial y^2}\right)$$

The stress function χ for the adhesive (I) is taken as follows[8] from solutions of variables separated of biharmonic functions under the boundary conditions of the stresses and the displacements generated in Step 2.

$$\chi = X_0 + X_1 + X_2$$
$$X_0 = k_1 xy + k_2 x^2 + k_3 y^2 + k_4 xy^2 + k_5 x^2 y + k_6 y^3$$
$$X_1 = \chi_1 + \chi_2 + \chi_3 + \chi_4$$

$$\chi_1 = \chi_1(\bar{A}_n, \bar{B}_s, l, h, \alpha_n, \lambda_s, \bar{\Delta}_n, \bar{\Omega}_s, x, y)$$
$$= \sum_{n=1}^{\infty} \frac{\bar{A}_n}{\bar{\Delta}_n \alpha_n^2} [\{\mathrm{sh}(\alpha_n l) + \alpha_n l \,\mathrm{ch}(\alpha_n l)\} \,\mathrm{ch}(\alpha_n x) - \mathrm{sh}(\alpha_n l)\alpha_n x \,\mathrm{sh}(\alpha_n x)] \cos(\alpha_n y)$$
$$+ \sum_{s=1}^{\infty} \frac{\bar{B}_s}{\bar{\Omega}_s \lambda_s^2} [\{\mathrm{sh}(\lambda_s h) + \lambda_s h \,\mathrm{ch}(\lambda_s h)\} \,\mathrm{ch}(\lambda_s y) - \mathrm{sh}(\lambda_s h)\lambda_s y \,\mathrm{sh}(\lambda_s y)] \cos(\lambda_s x)$$

$$\chi_2 = \chi_2(\bar{\bar{A}}_n, \bar{\bar{B}}_s, l, h, \alpha_n, \lambda_s, \bar{\bar{\Delta}}_n, \bar{\bar{\Omega}}_s, x, y)$$
$$= \sum_{n=1}^{\infty} \frac{\bar{\bar{A}}_n}{\bar{\bar{\Delta}}_n \alpha_n^2} [\{\mathrm{ch}(\alpha_n l) + \alpha_n l \,\mathrm{sh}(\alpha_n l)\} \,\mathrm{sh}(\alpha_n x) - \mathrm{ch}(\alpha_n l)\alpha_n x \,\mathrm{ch}(\alpha_n x)] \cos(\alpha_n y)$$
$$+ \sum_{s=1}^{\infty} \frac{\bar{\bar{B}}_s}{\bar{\bar{\Omega}}_s \lambda_s^2} [\{\mathrm{ch}(\lambda_s h) + \lambda_s h \,\mathrm{sh}(\lambda_s h)\} \,\mathrm{sh}(\lambda_s y) - \mathrm{ch}(\lambda_s h)\lambda_s y \,\mathrm{ch}(\lambda_s y)] \cos(\lambda_s x)$$

$$\chi_3 = \chi_3(\bar{A}_n, \bar{B}_s, l, h, \alpha'_n, \lambda'_s, \bar{\Delta}_n, \bar{\Omega}_s, x, y)$$
$$= \sum_{n=1}^{\infty} \frac{\bar{A}_n}{\bar{\Delta}_n \alpha_n'^2} [\{\mathrm{sh}(\alpha'_n l) + \alpha'_n l \,\mathrm{ch}(\alpha'_n l)\} \,\mathrm{ch}(\alpha'_n x) - \mathrm{sh}(\alpha'_n l)\alpha'_n x \,\mathrm{sh}(\alpha'_n x)] \sin(\alpha'_n y)$$
$$+ \sum_{s=1}^{\infty} \frac{\bar{B}_s}{\bar{\Omega}_s \lambda_s'^2} [\{\mathrm{sh}(\lambda'_s h) + \lambda'_s h \,\mathrm{ch}(\lambda'_s h)\} \,\mathrm{ch}(\lambda'_s y) - \mathrm{sh}(\lambda'_s h)\lambda'_s y \,\mathrm{sh}(\lambda'_s y)] \sin(\lambda'_s x)$$

$$\chi_4 = \chi_4(\bar{\bar{A}}_n, B_s, l, h, \alpha'_n, \lambda'_s, \bar{\bar{\Delta}}_n, \bar{\bar{\Omega}}_s, x, y)$$
$$= \sum_{n=1}^{\infty} \frac{\bar{\bar{A}}_n}{\bar{\bar{\Delta}}_n \alpha_n'^2} [\{\mathrm{ch}(\alpha'_n l) + \alpha'_n l \,\mathrm{sh}(\alpha'_n l)\} \,\mathrm{sh}(\alpha'_n x) - \mathrm{ch}(\alpha'_n l)\alpha'_n x \,\mathrm{ch}(\alpha'_n x)] \sin(\alpha'_n y)$$
$$+ \sum_{s=1}^{\infty} \frac{\bar{\bar{B}}_s}{\bar{\bar{\Omega}}_s \lambda_s'^2} [\{\mathrm{ch}(\lambda'_s h) + \lambda'_s h \,\mathrm{sh}(\lambda'_s h)\} \,\mathrm{sh}(\lambda'_s y) - \mathrm{ch}(\lambda'_s h)\lambda'_s y \,\mathrm{ch}(\lambda'_s y)] \sin(\lambda'_s x)$$

$$X_2 = \chi'_1 + \chi'_2 + \chi'_3 + \chi'_4$$

$$\chi'_1 = \chi'_1(\bar{A}'_n, \bar{B}'_s, l, h, \alpha'_n, \lambda'_s, \bar{\Delta}'_n, \bar{\Omega}'_s, x, y)$$
$$= \sum_{n=1}^{\infty} \frac{\bar{A}'_n}{\bar{\Delta}'_n \alpha_n'^2} \{\mathrm{ch}(\alpha'_n l)\alpha'_n x \,\mathrm{sh}(\alpha'_n x) - \alpha'_n l \,\mathrm{sh}(\alpha'_n l) \,\mathrm{ch}(\alpha'_n x)\} \cos(\alpha'_n y)$$
$$+ \sum_{s=1}^{\infty} \frac{\bar{B}'_s}{\bar{\Omega}'_s \lambda_s'^2} \{\mathrm{ch}(\lambda'_s h)\lambda'_s y \,\mathrm{sh}(\lambda'_s y) - \lambda'_s h \,\mathrm{sh}(\lambda'_s h) \,\mathrm{ch}(\lambda'_s y)\} \cos(\lambda'_s x)$$

$$\chi'_2 = \chi'_2(\bar{\bar{A}}'_n, \bar{\bar{B}}'_s, l, h, \alpha'_n, \lambda'_s, \bar{\bar{\Delta}}'_n, \bar{\bar{\Omega}}'_s, x, y)$$
$$= \sum_{n=1}^{\infty} \frac{\bar{\bar{A}}'_n}{\bar{\bar{\Delta}}'_n \alpha_n'^2} \{\mathrm{sh}(\alpha'_n l)\alpha'_n x \,\mathrm{ch}(\alpha'_n x) - \alpha'_n l \,\mathrm{ch}(\alpha'_n l) \,\mathrm{sh}(\alpha'_n x)\} \cos(\alpha'_n y)$$
$$+ \sum_{s=1}^{\infty} \frac{\bar{\bar{B}}'_s}{\bar{\bar{\Omega}}'_s \lambda_s'^2} \{\mathrm{sh}(\lambda'_s h)\lambda'_s y \,\mathrm{ch}(\lambda'_s y) - \lambda'_s h \,\mathrm{ch}(\lambda'_s h) \,\mathrm{sh}(\lambda'_s y)\} \cos(\lambda'_s x)$$

$$\chi'_3 = \chi'_3(\bar{A}'_n, \bar{B}'_s, l, h, \alpha_n, \lambda_s, \bar{\Delta}_n, \bar{\Omega}_s, x, y)$$
$$= \sum_{n=1}^{\infty} \frac{\bar{A}'_n}{\bar{\Delta}'_n \alpha_n^2} \{\mathrm{ch}(\alpha_n l)\alpha_n x \,\mathrm{sh}(\alpha_n x) - \alpha_n l \,\mathrm{sh}(\alpha_n l) \,\mathrm{ch}(\alpha_n x)\} \sin(\alpha_n y)$$
$$+ \sum_{s=1}^{\infty} \frac{\bar{B}'_s}{\bar{\Omega}'_s \lambda_s^2} \{\mathrm{ch}(\lambda_s h)\lambda_s y \,\mathrm{sh}(\lambda_s y) - \lambda_s h \,\mathrm{sh}(\lambda_s h) \,\mathrm{ch}(\lambda_s y)\} \sin(\lambda_s x)$$

$$\chi_4' = \chi_4'(\bar{\bar{A}}_n', \bar{\bar{B}}_s', l, h, \alpha_n, \lambda_s, \bar{\bar{\Delta}}_n, \bar{\bar{\Omega}}_s, x, y)$$
$$= \sum_{n=1}^{\infty} \frac{\bar{\bar{A}}_n'}{\bar{\bar{\Delta}}_n' \alpha_n^2} \{\mathrm{sh}(\alpha_n l)\alpha_n x \,\mathrm{ch}(\alpha_n x) - \alpha_n l \,\mathrm{ch}(\alpha_n l)\,\mathrm{sh}(\alpha_n x)\} \sin(\alpha_n y)$$
$$+ \sum_{s=1}^{\infty} \frac{\bar{\bar{B}}_s'}{\bar{\bar{\Omega}}_s' \lambda_s^2} \{\mathrm{sh}(\lambda_s h)\lambda_s y \,\mathrm{ch}(\lambda_s y) - \lambda_s h \,\mathrm{ch}(\lambda_s h)\,\mathrm{sh}(\lambda_s y)\} \sin(\lambda_s x) \tag{10}$$

where

$$\alpha_n = \frac{n\pi}{h}, \qquad \alpha_n' = \frac{2n-1}{2h}\pi, \qquad \lambda_s = \frac{s\pi}{l}, \qquad \lambda_s' = \frac{2s-1}{2l}\pi$$
$$\bar{\Delta}_n = \bar{\Delta}_n' = \bar{\Delta}_n(\alpha_n) = \mathrm{sh}(\alpha_n l)\,\mathrm{ch}(\alpha_n l) + \alpha_n l,$$
$$\bar{\bar{\Delta}}_n = \bar{\bar{\Delta}}_n' = \bar{\bar{\Delta}}_n(\alpha_n) = \mathrm{sh}(\alpha_n l)\,\mathrm{ch}(\alpha_n l) - a_n l$$
$$\bar{\Omega}_s = \bar{\Omega}_s' = \bar{\Omega}_s(\lambda_s) = \mathrm{sh}(\lambda_s h)\,\mathrm{ch}(\lambda_s h) + \lambda_s h$$
$$\bar{\bar{\Omega}}_s = \bar{\bar{\Omega}}_s' = \bar{\bar{\Omega}}_s(\lambda_s) = \mathrm{sh}(\lambda_s h)\,\mathrm{ch}(\lambda_s h) - \lambda_s h$$
$$\bar{\Delta}_n = \bar{\Delta}_n' = \bar{\Delta}_n(\alpha_n'), \qquad \bar{\bar{\Delta}}_n = \bar{\bar{\Delta}}_n' = \bar{\bar{\Delta}}_n(a_n'), \qquad \bar{\Omega}_s = \bar{\Omega}_s' = \bar{\Omega}_s(\lambda_s'),$$
$$\bar{\bar{\Omega}}_s = \bar{\bar{\Omega}}_s' = \bar{\bar{\Omega}}_s(\lambda_s'), \quad \mathrm{sh} : \sinh \quad \mathrm{ch} : \cosh$$

In Eq. (10), $k_1, \ldots, k_6$, $\bar{A}_n$, $\bar{\bar{A}}_n$, $\bar{A}_n$, $\bar{\bar{A}}_n$, $\bar{A}_n'$, $\bar{\bar{A}}_n'$, $\bar{A}_n'$, $\bar{\bar{A}}_n'$, $\bar{B}_s$, $\bar{\bar{B}}_s$, $\bar{B}_s$, $\bar{\bar{B}}_s$, $\bar{B}_s'$, $\bar{\bar{B}}_s'$, $\bar{B}_s'$, $\bar{\bar{B}}_s'$, $(n, s = 1, 2, 3, \ldots)$ are unknown coefficients. The unknown coefficients are determined by comparing the coefficients of both the stresses and the displacements transformed into Fourier series as was done in step 2. Thus, the stress function χ can then be selected. In addition, the stresses σ_r and $\tau_{r\theta}$ at the periphery of the circular hole $(r = a)$ are generated again and they are expressed by using the stress function χ and Eq. (8). The procedure of Steps 2 and 3 is continued until the boundary conditions shown in Eqs. (1), (2) and (3) are satisfied sufficiently, and finally the stresses and the displacements in adhesive(I) can be obtained.

3 EXPERIMENTAL METHOD

In order to measure the stress distribution on adherends and the adhesive shown in Fig. 3 were used in photoelastic experiments. A pure

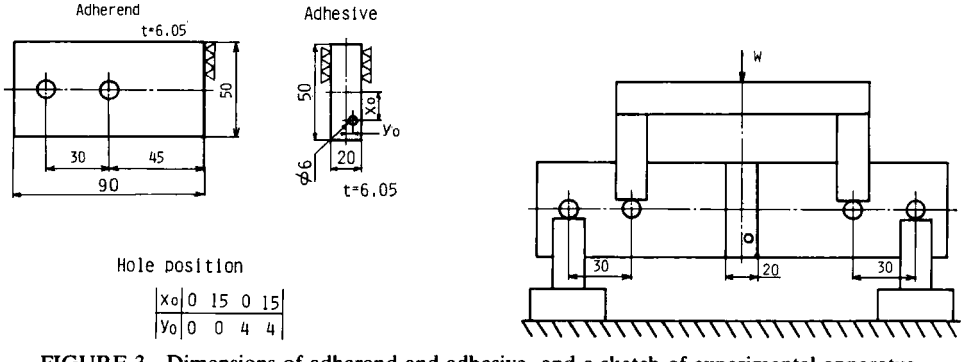

FIGURE 3 Dimensions of adherend and adhesive, and a sketch of experimental apparatus.

bending moment is applied to the joint using an apparatus shown in Fig. 3. The adhesive is made of epoxy resin and the adherend is made of steel for structural use (S45C, JIS). Young's modulus of steel (205 GPa) is about 60 times larger than that of epoxy resin (3.43 GPa) so that the adherends were considered to be relatively rigid.[11] The specimen thickness was 6.05mm and the bonded surfaces were finished by grinding. After bonding and curing, photoelastic experiments were performed. A pure bending moment (6.25 Nm) was applied to the joint by using a four-point-bending experimental system. The hole was made by milling and the residual stress was found to be 1.00N/mm^2. The specimens were heated gradually to 125°C in an hour and kept at the maximum temperature for 40 minutes. Then, they were cooled down gradually to 80°C in four hours and left in a furnace. After annealing, the residual stress of 1.00N/mm^2 was removed.

4 RESULTS AND CONSIDERATIONS

4.1 Principal stresses at the interface and at the hole periphery

In numerical calculations, the number of terms, N, of the series was taken as 40 and the alternating number as 15, using steps of <1% so that a satisfactory degree of convergence was expected. In order to estimate the strength of joints and the initiation point of fracture in the joint when the joints are subjected to external bending moments, the maximum principal stresses at the interface between the adherend and the adhesive and at the hole periphery were examined numerically. Figure 4 shows the stresses when the hole is at the center ($x_0 = y_0 = 0$) of the adhesive. In this figure σ_{yM} is the value of the stress σ_y (the

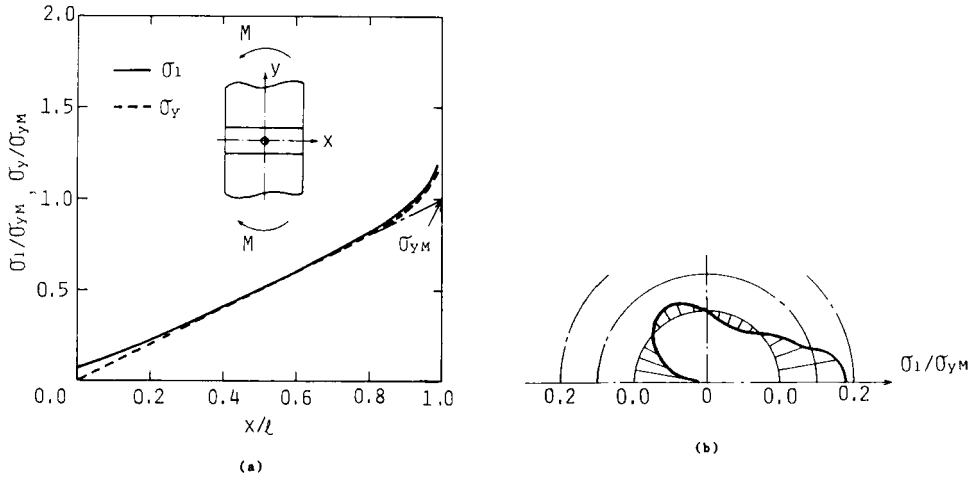

FIGURE 4 Distribution of stresses in the case where a hole is at the center: $x_0 = y_0 = 0$.
(a) at the interface ($y = \pm h$).
(b) at the hole periphery ($r = a$) [$h/l = 0.4$, $a/h = 0.3$].

dotted line) at $x = l$ which is supposed to be linearly distributed at the interface and which is expressed by an alternate long and short dash line. The maximum principal stress distribution at the interface is described by a solid line shown in Fig. 4(a). From this figure, it is seen that the maximum principal stress σ_1 is $1.14\sigma_{yM}$ near both ends, *i.e.* at $x = +0.98l$, because the stresses at both ends are singular. Similarly, the maximum principal stress distribution at the hole periphery is shown in Fig. 4(b). It is seen that the maximum principal stress σ_1 is $0.186\sigma_{yM}$ at both ends of the hole in the x-direction ($x = +0.12$, $y = 0$). Figure 5 shows the maximum principal stresses when the hole is shifted to the position of $x_0 = 0.6l$ and $y_0 = 0$. In both Fig. 5(a) and (b), the maximum principal stresses distribute asymmetrically to the y-axis, and the maximum stresses σ_1 are $1.22\sigma_{yM}$ and $1.68\sigma_{yM}$ near the edge of the interface ($x = 0.98l$, $y = +h$) and at the end of the hole in the direction of the hole shift ($x = 0.72l$, $y = 0$), respectively. The maximum principal stress at the periphery of the hole is larger than that at the interface between the adherend and the adhesive when the hole shifts to the x-direction. Taking account of the stress singularity at the interface, it is difficult to predict the first position where a fracture will be caused, but it is seen that the maximum principal stress at the hole periphery has an influence on the bending strength of the adhesive joint.

4.2 The relationship between the hole position and the maximum principal stress

Figure 6 shows the stress distribution (σ_y/σ_{yM}) of an adhesive at $y = 0$ in the x-direction when a joint has a hole at the center of the adhesive. It is seen that the stress σ_y at the hole periphery equals $0.18\sigma_{yM}$. Figure 7 shows the stress distribution (σ_y/σ_{yM}) at $y = 0$ in the x-direction when a joint has a hole at the

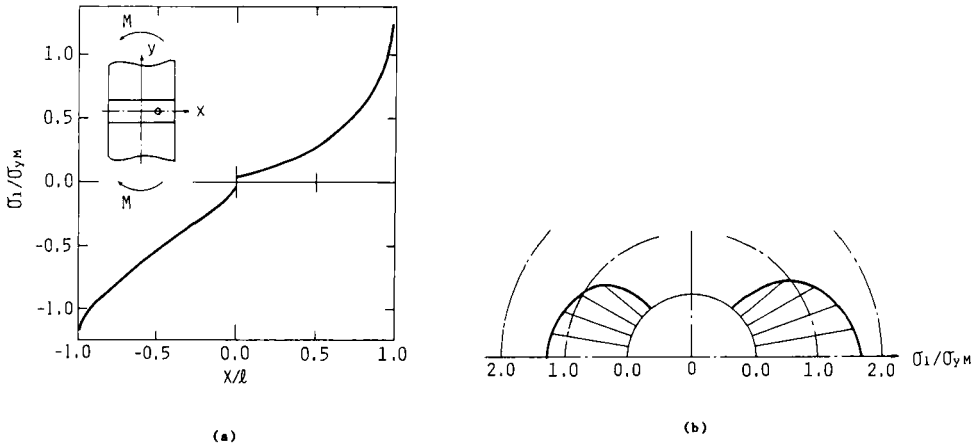

FIGURE 5 Distribution of maximum principal stress in the case where a hole is at $x_0 = 0.6l$, $y_0 = 0$.
(a) at the interface ($y = \pm h$)
(b) at the hole periphery ($r = a$) [$h/l = 0.4$, $a/h = 0.3$].

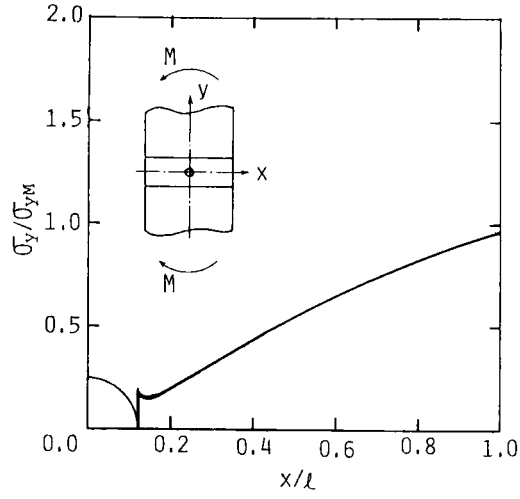

FIGURE 6 Stress distribution σ_y when a hole is at the center: $x_0 = y_0 = 0$. [$y = 0$, $h/l = 0.4$, $a/h = 0.3$].

position of $x_0 = 0.6l$ and $y_0 = 0$ in the adhesive. In this case, the stress increases at both ends of the hole ($x = 0.48l$, $y = 0$ and $x = 0.72l$, $y = 0$). However, the stress σ_y becomes maximal at the hole periphery ($x = 0.72l$, $y = 0$) which is close to the free surface of the adhesive. By numerical calculation, this was found to be $1.68\sigma_{yM}$. Furthermore, when the hole shifts to the position of $x_0 = 0$ and $y_0 = 0.4h$, the stress distribution σ_y is much the same as in the case of Fig. 6. The

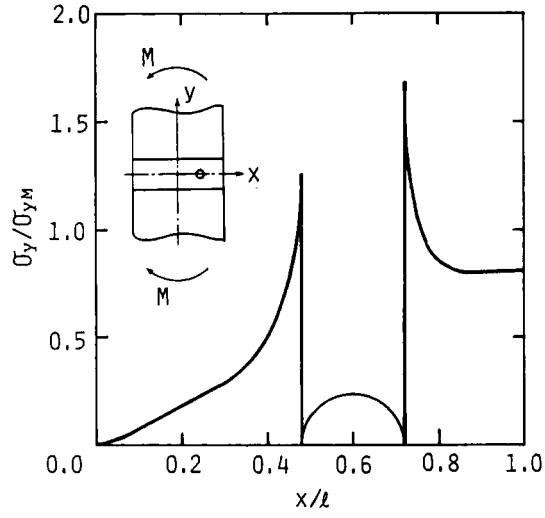

FIGURE 7 Stress distribution σ_y when a hole is at $x_0 = 0.6l$, $y = 0$. [$y = 0$, $h/l = 0.4$, $a/h = 0.3$].

value of the stress σ_y is $0.18\sigma_{yM}$ at the hole periphery ($x = +0.12l$, $y = 0.4h$). When the hole shifts to the position of $x_0 = 0.6l$ and $y_0 = 0.4h$, the stress σ_y becomes maximal at the hole periphery ($x = 0.72l$, $y = 0.4h$), as was the case for Fig. 7. The value of σ_y becomes $1.61\sigma_{yM}$; however, it is slightly smaller than that of the case when the hole shifts in the x-direction only. It is seen that the stress σ_y in the case where the hole is on the x-axis is larger than that in the case where it shifts in the y-direction. Figure 8 shows the relationship between the maximum principal stress and the hole position in the x-direction of the adhesive. The solid line represents the case where the hole radius a is $0.12l$, and the dotted line the case where the hole radius a is $0.012l$. From this figure, it is seen that the maximum principal stress increases with an increase of the shift of the hole to the free boundary of the adhesive, *ie.* it is significantly larger than 2.09 σ_{yM} in the case where the hole is at the position of $x_0 = 0.8l$ and $y_0 = 0$ and the hole radius a is $0.12h$.

4.3 Effect of the size of the hole

In practice, adhesive joints probably contain holes (microdefects) of various size in the adhesive layer. Hence, the effect of hole size on the principal stress at the periphery of the hole located at the center of the adhesive ($x_0 = y_0 = 0$), was examined numerically. The analytical result is shown in Fig. 9. In this figure, the abscissa is the ratio a/l of the hole radius to the half-width of the adhesive and the ordinate is the stress σ_1/σ_{yM}. The solid line represents the case where the ratio h/l of the thickness to the half-width of the adhesive is 0.4, and the dotted line the case where the ratio is 0.2, and the alternate long and short dash line the case where the ratio is 0.04. From this figure, it is seen that the maximum principal

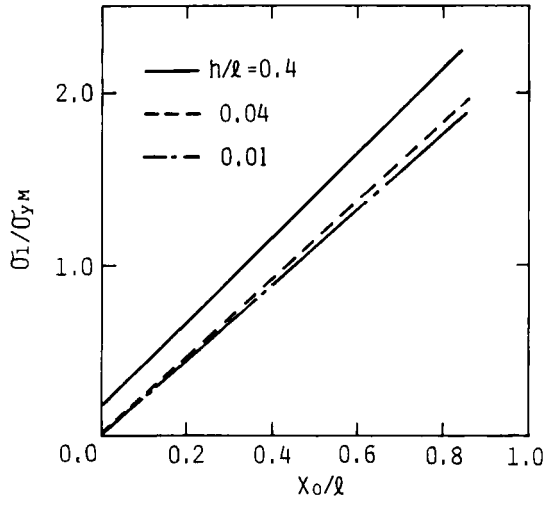

FIGURE 8 Relationship between hole position and maximum principal stress at the hole periphery. [$y = 0$, $a/h = 0.3$].

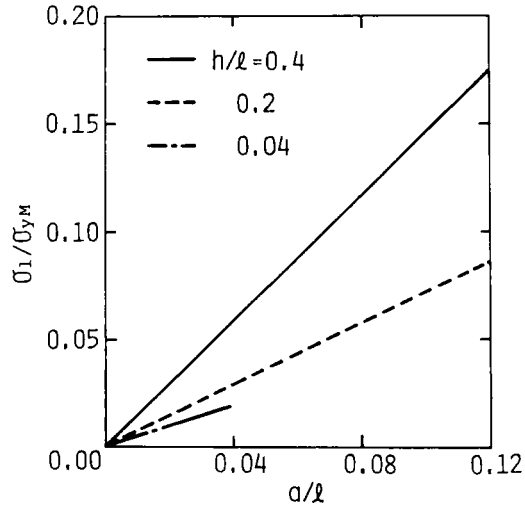

FIGURE 9 Relationship between ratio a/l and maximum principal stress at the hole periphery. $[(x_0, y_0) = (0, 0)]$.

stress increases with an increase in the hole radius (ie., the strength of the joint decreases relatively with an increase in the hole radius). In addition, the maximum principal stress tends to decrease with a decrease of the thickness of the adhesive.

4.4 Stress distribution near the edge of the interface

Figure 10 shows the relationship between the maximum principal stress σ_1/σ_{yM} and the distance r from the edge of the interface on a logarithmic scale.[12] This

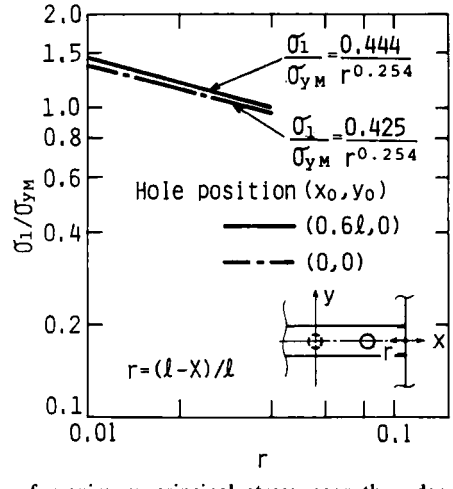

FIGURE 10 Distribution of maximum principal stress near the edge of the interface indicated on logarithmic scales.
$[y = \pm h,\ h/l = 0.4,\ a/h = 0.3]$.

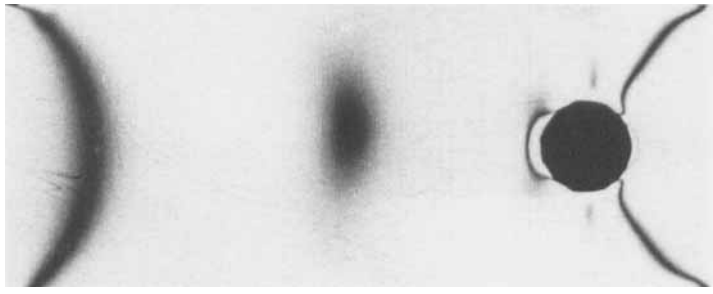

FIGURE 11 An example of experimental results obtained by photoelasticity. A hole is at $x_0 = 15$ mm and $y_0 = 0$.

figure is presented in order to examine the property of the stress singularity at the close vicinity of a bonding edge, as in the case of Figs. 4 and 5. Generally, the maximum principal stress σ_1 near the point where a stress singularity is caused is expressed approximately by Eq. (11).

$$\sigma_1(r) = K/r^{\lambda} \tag{11}$$

where

$\sigma_1(r)$ Maximum principal stress.
r Distance from singular point.
K Intensity of stress singularity.
λ Order of stress singularity.

The parameter λ is determined by the method demonstrated in References 12 and 13. In this paper, r is taken to be 0.04 and r is expressed by the equation $r = (l - x)/l$. Determining the value of K from the distribution indicated on a

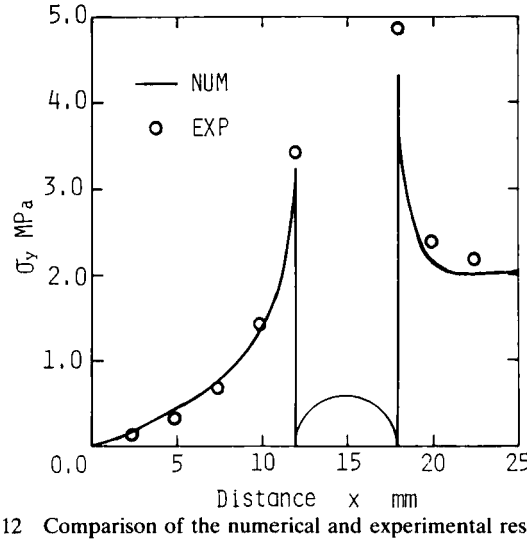

FIGURE 12 Comparison of the numerical and experimental results ($y = 0$).

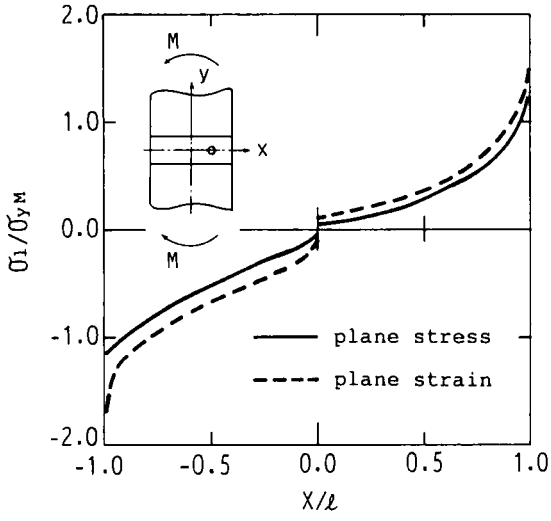

FIGURE 13 Comparison between the numerical result in plane stress and that in plane strain.

logarithmic scale, the equations for σ_1 are expressed in Fig. 10 for the case of the hole positions $(x_0, y_0) = (0, 0)$ and $(0.6l, 0)$.

4.5 Comparison of the numerical results with the experimental results

Figure 11 shows an example of the experimental results obtained by photoelasticity. Figure 12 shows the stress distribution σ_y at $y = 0$ in the x-direction in the case where the joint has a hole at the position $x_0 = 15$ mm and $y_0 = 0$ in the adhesive. In numerical calculations, Young's modulus and Poisson's ratio of the adhesive are put as 3.43 *GPa* and 0.376, respectively. The ordinate is the stress σ_y and the abscissa is the distance x from the center of the adherend. The solid line and the open circles represent the numerical and experimental results, respectively. It is seen that the numerical results are fairly consistent with the experimental results. Figure 13 shows the comparison between the numerical results in the case of plane stress and in the case of plane strain. The maximum stress is greater in plane strain than that in plane stress.

5 CONCLUSIONS

This paper dealt with a stress analysis of a butt adhesive joint having a circular hole in the adhesive when the joint was subjected to an external bending moment, in order to clarify the effects of a hole on the strength of the joint. For verification, photoelastic experiments were performed. The results obtained are as follows.

(1) A method of analysis was demonstrated by using a two-dimensional theory of elasticity (plane stress) in order to obtain the stress distribution in the adhesive.
(2) It was seen that a stress singularity was caused at the edge of the interface and a stress concentration was also caused at the periphery of the hole. Fracture was expected to occur at either of these two points.
(3) A stress concentration was caused at the hole periphery when an external bending moment was applied, and the maximum stress varied with the position of the hole. When the hole was shifted in the direction of adhesive thickness, the value of the maximum stress decreased; when the hole was shifted in the direction of adhesive width, it increased linearly with an increase in the shift of the hole.
(4) It was seen that the stress concentration at the hole periphery became larger with an increase of the size of a hole.
(5) The stress distribution in the adhesive was measured by photoelastic experiments, and it was shown that the analytical results were fairly consistent with the experimental results obtained by photoelasticity.

References

1. R. M. Baker and F. Hatt, *AIAA J.* **11,** 1650(1973).
2. J. K. Sen and R. M. Jones, *AIAA J.* **18,** 1376 (1980).
3. R. D. Adams, J. Coppendale, and N. A. Peppiatt, *J. Strain Anal.* **13,** 1 (1978).
4. F. Erdogan, and M. Ratwani, *J. Composite Materials* **5,** 378 (1971).
5. T. Wah, *Int. J. Mech. Sci.* **18,** 223 (1976).
6. W. J. Renton, *J. Adhesion* **10,** 139 (1979).
7. T. Sawa, Y. Nakano and K. Temma, *J. Adhesion* **24,** 1 (1987).
8. Y. Nakano, K. Temma, and T. Sawa, *JSME. Int. J.* **31,** 507 (1988).
9. C. L. Chow, C. W. Woo, *Int. Congr. Exp. Mech.* **1984,** 256 (1984).
10. S. P. Timoshenko, and J. N. Goodier *Theory of Elasticity* [*3rd ed*] (McGraw-Hill, New York, 1970), p. 65.
11. T. Sawa, A. Iwata, and H. Ishikawa, *Bull. JSME* **29,** 4037 (1986).
12. T. Hattori, S. Sakata, T. Watanabe, *Advances in Adhesively Bonded Joints,* (1988), The Annual Winter Meeting of ASME, p. 43.
13. D. B. Bogy, *J. Appl. Mech* **38,** 377 (1971).